Closed-loop feedback control and bifurcation analysis of epileptiform activity via optogenetic stimulation in a mathematical model of human cortex

Prashanth Selvaraj, Jamie W. Sleigh, Heidi E. Kirsch, and Andrew J. Szeri

Phys. Rev. E **93**, 012416 — Published 26 January 2016

DOI: 10.1103/PhysRevE.93.012416

Closed loop feedback control and bifurcation analysis of epileptiform activity via optogenetic stimulation in a mathematical model of human cortex

Prashanth Selvaraj,[1,*] Jamie W. Sleigh,[2] Heidi E. Kirsch,[3] and Andrew J. Szeri[1,4,†]

[1]*Department of Mechanical Engineering,*
University of California, Berkeley, CA 94720-1740, USA
[2]*Waikato Clinical School, University of Auckland, Hamilton, New Zealand*
[3]*Departments of Neurology and Radiology and Biomedical Imaging,*
University of California, San Francisco, CA 94143, USA
[4]*Center for Neural Engineering and Prostheses,*
University of California, Berkeley, CA 94720-3370, USA

Abstract

Optogenetics provides a method of neuron stimulation that has high spatial, temporal and cell type specificity. Here we present a model of optogenetic feedback control that targets the inhibitory population, which expresses light sensitive Channelrhodopsin-2 (ChR2) channels, in a mean field model of undifferentiated cortex that is driven to seizures. The inhibitory population is illuminated with an intensity that is a function of electrode measurements obtained via the cortical model. We test the efficacy of this control method on seizure like activity observed in two parameter spaces of the cortical model that most closely correspond to seizures observed in patients. We also compare the effect of closed loop and open loop control on seizure like activity using a less complicated ordinary differential equation (ODE) model of the undifferentiated cortex in parameter space. Seizure like activity is successfully suppressed in both parameter planes using optimal illumination intensities less likely to have adverse effects on cortical tissue.

* pselvaraj@berkeley.edu
† aszeri@berkeley.edu

I. INTRODUCTION

The different etiologies of seizures make diagnosis and treatment of this disorder complicated tasks. Physical trauma, stroke and tumors are examples of causes that may be more easily identifiable than those responsible for idiopathic seizures. However, despite the differences in etiologies, all epileptic seizures are characterized by the excessive synchronous firing of a large number of neurons [1]. This activity is captured well at the mesoscale, which involves the averaged activity of millions of neurons. Electroencephalography (EEG), which is one of the most helpful tests to identify idiopathic seizures [2], and electrocorticography (ECoG), are two techniques used to observe cortical activity at this scale.

To simulate cortical activity at the mesoscale, Liley at el. [3] proposed a mathematical model of the cortex based on the columnar arrangement of cortical neurons, which was first discovered by Santiago Ramón y Cajal towards the end of the 19th century. Since then, this mesoscale model of the cortex has been shown to model the mesoscopic electrical behavior recorded from the human cortex during sleep [4, 5, 7], anaesthesia [9] and seizures [10–12]. Various methods of feedback control were demonstrated to suppress seizures simulated using the cortical model [13], which resulted in a biologically relevant method of closed loop control [14] to treat medically refractory epilepsy. Modulation of traveling waves, as seen in [11], was also carried out experimentally in [15], while the efficacy of feedback control in suppressing seizures was experimentally demonstrated in [16] in hippocampal brain slices.

Optogenetics offers another modality of seizure control, albeit with higher spatial, temporal and cell type specificity than any other method of stimulation [17]. Open loop optogenetic control of a seizing model human cortex has already been demonstrated [11] using a model of channelrhodpsin-2 (ChR2) dynamics [18]. ChR2 is a cation pump that is activated by blue light of maximum wavelength 480 nm [19]. Closed loop control of epileptiform activity using optogenetics has been experimentally demonstrated in rats [20, 21] and in mice [22]. Here, we investigate a method of closed loop feedback control using the proportional integral (PI) mode of control. By basing our control strategy on electrode measurements of the same spatial and temporal scales as the cortical model, we propose a method of seizure inhibition that is biologically relevant and efficient in the use of energy required to effect control - criteria that have to be satisfied for the use of any control strategy in humans over long periods of time. We also study seizures in two parametric spaces of the cortical model that most closely correspond

to seizures observed in patient data. Comparisons between open loop and closed loop control, and the effect of each method in suppressing seizures is studied using a simpler ordinary differential equation (ODE) model of the combined cortico-optogenetic dynamics, which is shown to correspond well with the full stochastic partial differential equations (SPDEs) that describe the dynamics of the model cortex. A bifurcation analysis of the combined cortico-optogenetic model in the open loop format and a time integration in the closed loop format are performed to study the hyperexcited cortical model's behavior when coupled with optogenetic stimulation.

This paper is organized as follows. First, we present a version of optogenetic PI control that uses electrode measurements of model cortical activity to calculate the intensity of light used to illuminate inhibitory neurons, which then depolarize and suppress excessive excitatory activity characteristic of epileptic seizures. **Next, we explore the efficacy of this control method in the parameter space defined by two parameters of the cortical model - the excitatory subcortical inputs (P_{ee}) and the influence of excitatory synaptic input on the mean soma potential (Γ_e), which acts as an amplitude gain that determines the strength of the excitatory inputs to a cell population. These parameters will be defined in detail in sections III and V, while the mathematical model describing cortical dynamics is presented in full in the appendix**. A simpler ODE system is used to perform a bifurcation analysis on the cortical model, and the combined cortico-optogenetic model in the open loop format, while a time stepping continuation is performed on the discontinuous closed loop model. **Finally, we explore the effect of closed loop PI control on seizures in the parameter space defined by two additional parameters of the cortical model - the slope (M_e) at the inflection point of the sigmoid function that describes the mean excitatory firing rate, and the influence of inhibitory synaptic input on the mean soma potential (Γ_i), which acts as an amplitude gain that determines the strength of the inhibitory inputs to a cell population.**

II. CLOSED LOOP OPTOGENETIC CONTROL

The use of optogenetics as an effective control modality for cortical seizures has been demonstrated in the context of a mathematical model in [11]. The inhibitory population of neurons in the mesoscale cortical model first developed by Liley [3] was modified to express light sensitive Channelrhodopsin-2 (ChR2) ion channels following the work of Grossman et al.[18]. When illuminated with light of wavelength 480 nm, these ion channels pump cations

into neurons, depolarising them. The ion conductance of ChR2 is dependent on the intensity of light used, and the membrane potential of the cell population expressing these channels. For convenience, we restate the equations describing optogenetic channel dynamics presented in [11].

$$\frac{dN_{O1}}{dt} = K_{a1}.N_{C1} - (K_{d1} + e_{12}).N_{O1} + e_{21}.N_{O2} \tag{1}$$

$$\frac{dN_{O2}}{dt} = K_{a2}.N_{C2} + e_{12}.N_{O1} + (K_{d2} + e_{21}).N_{O2} \tag{2}$$

$$\frac{dN_{C2}}{dt} = K_{d2}.N_{O2} - (K_{a2} + K_r).N_{C2} \tag{3}$$

$$N_{C1} = 1 - N_{O1} - N_{O2} - N_{C2} \tag{4}$$

Optogenetic dynamics occur at the cell level, which is at the microscale. However, we are interested in cortical dynamics at the mesoscale level. To adapt the optogenetic model to the meso scale, the values of N_{Oi} and N_{Ci} have been normalized with the total number of ChR2 channels per representative neuron, and now represent the fraction of channels in each state per representative neuron. The sum of these fractions equals unity, and is described in equation 4. Equations 1-3 describe the number of channels in the open and closed states, represented by N_{O1}, N_{O2}, and N_{C2}. The number of channels per unit area is obtained by multiplying the expression density with the fraction of each channel. Here, we use an expression density of $\sim 10^9/m^2$, which enables the use of light intensities that correspond to experiments [23]. Channel opening and closing rates are represented by the K and e terms. K_{ai} are the rates of transition from the closed states, $C1$ and $C2$, to the open states $O1$ and $O2$, respectively, and are dependent on the intensity of light illuminating the channels [11]. Conversely, K_{di} are the closing rates from the open states to the closed states, while K_r is the thermal recovery rate from $C2$ to $C1$. Both of these rates are assumed to be constants. e_{12} and e_{21} are the transition rates from $O1$ to $O2$ and vice versa, and are also dependent on the illumination intensity. **The values for all rate constants can be found in Appendix B.**

The total conductivity of ChR2 channels expressed by a neuron population in a cortical macrocolumn is given by,

$$G_{ChR2} = G_{max} \cdot g_{ChR2} . \frac{(1 - exp(-h_i/U_0))}{h_i/U_1}, \tag{5}$$

where h_i is the mean soma potential for the inhibitory population, G_{max} is the maximum conductance of optogenetic channels in the $O1$ state and has a value of 500 pS, g_{ChR2} is the total conductance of the optogenetic channels in the $O1$ and $O2$ states defined by $(N_{O1} + s_g.N_{O2})$, where s_g is the empirically derived ratio of channel conductivity in the $O1$ state to the $O2$ state with a value of 0.5. U_0 and U_1 are empirical constants with values of $40mV$ and $15mV$ respectively. Further explanation of the variables and the equations can be obtained in [11, 18].

From equations 1-3 and 5, we see higher channel opening rates, which in turn yield higher conductances, while higher **inhibitory mean soma** potentials reduce conductivity of these ion channels. Channel conductivity is dramatically reduced as the reversal potential of the neuron population is approached because of its dependence on the mean soma potential. External modulation of the conductance of these channels is thus only possible via the intensity of light illuminating the channels.

In [11], optogenetic control was used in an open loop configuration, where a pre determined intensity of light was chosen to illuminate the model cortex. If a high enough intensity is used, seizures are successfully inhibited. However, this does not result in optimal use of light energy, which is important for optogenetic control to be efficient and cost-effective. Additionally, prolonged exposure to high intensities of light has been shown to cause irreversible tissue damage in animal models [23], so we have to minimise the time the cortex is illuminated with high intensities to accommodate tissue safety concerns. In light of this, we propose a method of feedback control that satisfies these requirements.

A. Development of the control law

To design a feedback loop that provides optimal optogenetic stimulation, the light intensity has to be based on a measured variable in the combined cortical-optogenetic model. We have chosen to use the signal sensed at the surface of the cortex by an electrode, $\tilde{h}_m$ [14], for two reasons. Firstly, the length scales involved in the meso-scale model of the cortex used here are similar to the sizes of commercial electrode arrays. Secondly, it is a mean-field model, which means all variables in the model are spatially averaged properties of neuron popula-

tions. EEG/ECoG measurements are based on the ensemble behavior of many neurons, and the mesoscale model is suited to capturing such behavior.

The measured signal from the surface of the cortical model, $\tilde{h}_m$, is a function of the extracellular currents in the tissue, and not of the intracellular soma potential [24]. Taking this into account, Lopour et al. [14] defined $\tilde{h}_m$ using the following two equations:

$$\tilde{h}_m = (h_0^e - \tilde{h}_e)\tilde{I}_m \tag{6}$$

$$\begin{aligned}\left(\frac{1}{T_m}\frac{\partial}{\partial \tilde{t}} + 1\right)^2 \tilde{I}_m = F(&-0.413 \times N_e^\beta \tilde{S}_e - 0.092 \times N_i^\beta \tilde{S}_i \\ &- 0.458 \times \tilde{\phi}_e + 0.034 \times (P_{ee} + \tilde{\Gamma_1}) - 0.004 \times (P_{ie} + \tilde{\Gamma_3}))\end{aligned} \tag{7}$$

where $\tilde{h}_m$ is the potential measured by a cortical surface electrode, $\tilde{I}_m$ is the current measured at the cortical surface, h_0^e is the reversal potential of the excitatory population, $N_{e,i}^\beta$ are the number of synaptic connections from the excitatory and inhibitory populations, respectively, $\tilde{S}_{e,i}$ are the firing rates of the excitatory and inhibitory populations, respectively, P_{ee} and P_{ie} are the subcortical inputs from the excitatory and inhibitory populations to the excitatory population, and $\tilde{\phi}_e$ is the long range corticocortical input from the excitatory population. Please see appendix A for the full set of equations that describe the dynamics of the meso-scale cortical model and associated parameters. F is a positive gain parameter that helps convert the right side of equation 7, which is based on voltages, to currents, which is the basis of the left side of the equation. It also scales the magnitude of the synaptic inputs to ensure an appropriate amount of influence over the electrode measurement $\tilde{I}_m$. In equation 7, we use $F = 10^{-3}$. Throughout this paper, tildes are used to denote non-dimnesionalised variables in the meso-scale cortical model. Additionally, we include the mean offset of the measured signal, which gives us a net positive signal. This is in contrast to EEG readings, for example, where the mean offset is subtracted to obtain a signal with mean zero. The theory behind the measured signal, mean offset, equations 6 and 7, and the constants, coefficients and parameters used in these equations is explained in detail in [14].

To calculate intensity, E, that should enable successful control - i.e. the 'control law'- we use the concept of proportional and integral (PI) control. As we are dealing with a highly non-linear and stochastic system, PI control offers a simple, but effective way to calculate the control effort based on the measured potential $\tilde{h}_m$:

$$E = K_P \tilde{h}_m + K_I \int_{t-d\tau}^{t} \tilde{h}_m dt \tag{8}$$

The first term of eq. 8 represents proportional control, where K_P is proportional gain. This component of the control effort calculates a contribution to the intensity of light to be used based on the current value of measured potential. Spikes in intensity with highs past the physiological limit, and lows tending to zero, will lead to unsafe and ineffective control. To avoid this, we lower K_P to ensure peak values of intensity are safe for cortical tissue, and add a second term based on the integral of $\tilde{h}_m$ over a short duration of time, $d\tau$. Throughout this manuscript, we use $d\tau = 0.2$s, which is the most optimal amount of time to integrate over for the integral control term, while also maintaining computational efficiency. This contribution is modulated by K_I, which is the integral gain term in eq. 8, and addresses shortfalls in intensity, and synaptic delays between cell populations, that lead to continued seizure activity.

It should be noted that equation 8 is slightly different from the traditional form of PI control, where the control effort is based on minimising the error in the measured signal. Error would be calculated based on the difference between amplitude of the expected signal and the measured signal. However, the mathematical model of the human cortex consists of a highly stochastic, non-linear system of PDEs, and in the example simulations we present in the paper, the values of parameters associated with the model change over time - e.g. P_{ee} varies with time. This leads to a non-stationary expected value of $\tilde{h}_m$. However, the expected value of $\tilde{h}_m$ in a normally functioning cortex is much smaller than peak $\tilde{h}_m$ values observed during the seizure state. We can thus neglect the estimated value and calculate control effort based directly on the measured variable $\tilde{h}_m$.

The entire spatial domain of the model cortex is discretized with a Cartesian mesh to perform numerical simulations. The measured potential and intensity are calculated as piecewise constant approximations at every grid point, and we do not account for the electrodes' spatial profiles, or the spatial variation of illumination in this first study of the efficacy of the control law and the dynamics of the combined cortico-optogenetic model during closed loop stimulation.

B. Optogenetic inhibition

Certain inhibitory neuron types and neural circuits might be responsible for cortical disorders and play an integral role in cortical function. For example, GABAergic inhibition is decreased

in some types of epilepsy [39, 40]. The targeted stimulation of this specific class of inhibitory neurons is one possible way to address this decrease in inhibition. The meso-scale model we use in this work does not include specific subtypes of inhibitory neurons, but it does allow us to explore the efficacy of optogenetic depolarisation of the inhibitory neuron population.

Additionally, the distribution of inhibitory neurons in mammalian cortices is non-uniform, with the majority of inhibitory neurons embedded well below the cortical surface [43]. Targeted stimulation of neurons at or near the surface of the cortex only has a distinct effect on pyramidal (excitatory) neurons [14] while ignoring a large range of stimulation options via inhibition. However, [23] and [42] have shown light can penetrate at least 1 mm or more beneath the cortical surface giving access to a number of other neuron types that can be found in larger numbers in layers 2-6 of the cortex.

First in [13] and then in [11], the model cortex was hyperexcited by increasing the excitatory subcortical inputs to a magnitude 50 times higher than during normal function. This led to traveling seizure waves that were suppressed in [11] by optogenetic control, which was applied by depolarising inhibitory neurons that express ChR2 channels to increase inhibition. However, the measured potential, $\tilde{h}_m$, is related to the mean soma potential of the excitatory population, $\tilde{h}_e$, because surface electrode measurements are averaged readings from apical dendrites of pyramidal neurons, which are excitatory in nature. This means the light intensity required to illuminate the inhibitory population is also most closely related to $\tilde{h}_e$. In essence, to apply control, we measure the activity of the excitatory population, calculate intensity based on this measurement, which is then used to stimulate the inhibitory population. The effect of control is then measured again via the excitatory population and adjustments to the illumination intensity are made until seizures are suppressed.

C. Triggering and deploying control

Numerous methods of seizure detection using EEG/ECoG signals have been proposed over the last few years. Orosco et al. [25] used energy thresholds of instantaneous frequency data to detect seizures with around 60% accuracy. Spike features such as amplitude, width, rate and regularity, and changes in energy within specific frequency bands were taken into account while developing a seizure detection algorithm by Krook-Magnusson et al. [22]. Neural networks [26], entropy estimators [27], and a combination of neural networks and an entropy estimator

[28] have been trained to detect seizures with more than 90% accuracy. The different methods currently available for seizure detection, and the pathway from acquiring data to closed loop applications can be found in [29]. Seizure prediction, on the other hand, has proven to be a more complicated task. Dynamical entrainment [30], accumulated signal energy [31] and phase synchronisation [32] are only a few examples of features of EEG data that were used in seizure prediction, but a fully satisfactory approach remains elusive. Realistically, given the wide variation in seizure pathologies and seizure types, a more subjective approach to detection [33] is required. This may entail a combination of detection methods including, but not limited to, electrode measurements, accelerometers, electrodermal activity and so on.

The aim of this work is to demonstrate the ability to calculate illumination intensity for optogenetic control directly from electrode measurements of cortical activity. The detection method merely serves as a trigger to turn on the controller, and does not play a role in the 'control law' itself. Here, we use a very straightforward trigger for seizure control based on the amplitude and rate of change of the measured potential, $\tilde{h}_m$, which has a mean value close to 0 during normal function, with fluctuations in amplitude that are much less than 0.1 in magnitude. Seizure activity is characterized by high amplitude oscillatory changes in the mean soma potential of neuron populations, and by extension, in $\tilde{h}_m$ as well. The amplitude and rate of change of amplitude thresholds that have to be surpassed for control to be triggered are based on the sensitivity of the controller, which in turn can be tuned differently for different paths to seizures. Again, this method of detection works well for the model seizures that we investigate in this work, but one can substitute any other detection method in its place to trigger the controller.

When control is triggered, the intensity of illumination is calculated based on the control law described in eq. 8. The proportional component contributes to changes in illumination intensity based on instantaneous changes in $\tilde{h}_m$, while the integral component is calculated over the past $d\tau$ seconds and changes more gradually. The integral part of the control provides an offset for the proportional component resulting in the optimal amount of light intensity being used to inhibit seizures.

We have also included an off switch for the controller, which is based on the illumination intensity E and the amplitude of the measured potential h_m. This is a straightforward switch similar to the trigger used to turn on the controller, and facilitates studying the efficacy of the controller. One could substitute other switches in its place, which would work just as well with the controller.

D. Tuning the controller

In the next two sections, we demonstrate the efficacy of the PI controller for seizures in two different parameter spaces. The first space is associated with subcortical inputs from the excitatory populations (P_{ee}) and the influence of excitatory synaptic inputs on the mean soma potential (Γ_e). The second space is defined by the slope at the inflection point of the mean firing rate (M_e) and the influence of inhibitory synaptic inputs on the mean soma potential (Γ_i). Please see appendix A for the full set of equations that describe the dynamics of the meso-scale cortical model. In separate work, these parameter spaces were identified as being the most probable regions in which seizures produced using the mesoscale model have been shown to be directly, and quantifiably, compared with electrocorticogram (ECoG) readings of seizures from a human subject [34].

In both parameter spaces, seizures are induced in a normally functioning model cortex by gradually varying one of the parameters with time. In both parameter spaces, the model cortex produces the most robust seizures at the peak value of these parameters. Both $d\tau$ and the gains of the PI controller, and the intensity for a comparable open loop controller, in turn, are tuned to suppress seizures induced at these peak values of the parameters.

Given the stochastic nature of the model cortex, we use numerical optimization to obtain the most optimal values of proportional and integral gains that successfully suppress seizures. We use the illumination intensity to define a cost function,

$$Cost = \int_{t_{on}}^{t_{off}} E dt \tag{9}$$

where E is the illumination intensity, t_{on} is the time at which control is switched on, and t_{off} is the time at which control is switched off. The cost, in terms of J/mm^2 is calculated for a range of proportional and integral gain terms. The response diagram for each pair of proportional and integral gains is examined for oscillations, and the pair which minimizes the total energy calculated by equation 9 while successfully suppressing seizures is chosen to calculate the control effort.

III. SEIZURES IN THE P_{ee}-Γ_e SPACE

Seizures in this parameter space are simulated by increasing subcortical inputs that will lead to a hyperexcited model cortex, while simultaneously reducing the influence of excitatory synaptic input on the mean soma potential. We will explore seizures caused by a decrease in inhibition in section V. An increase in subcortical inputs from the excitatory population, P_{ee}, leads to an increase in the post synaptic activation due to excitatory inputs ($\tilde{I}_{ee}$), which in turn increases the mean soma potential of both the excitatory ($\tilde{h}_e$) and inhibitory ($\tilde{h}_i$) cells that leads to higher firing rates in both populations. The post-synaptic activation due to the excitatory population in the seizing model cortex is lowered, while the post-synaptic activation due to the inhibitory population is held constant. This causes a net decrease in the post-synaptic influence of the excitatory population on itself and the inhibitory population. In addition, there are fewer inhibitory synapses than excitatory ones, leading to a net increase in excitation due to the hyper-excitatory subcortical inputs, that results in seizures in the model cortex. A more detailed analysis of the feedback and reciprocal synaptic connections in the model cortex that lead to seizures due to an increase in sub-cortical excitation can be found in [13].

When results from simulating cortical activity using the mesoscale model were compared with patient data [10], the magnitude of P_{ee} required to produce seizure like activity in the model cortex was almost 50 times the value of P_{ee} required for normal function. Here, we present two cases of epileptic seizures caused by excessive excitation with different values of Γ_e, the influence of the excitatory post-synaptic potential on the mean soma potential of a neuron population, and α, the amplitude of noise in the stochastic subcortical inputs. Please refer to the appendix for details about the noise in the stochastic inputs. The first case uses $\Gamma_e = 0.0008$ and $\alpha = 1.6$, while the second case uses $\Gamma_e = 0.00066$ and $\alpha = 1.15$. These parameter values are within the physiologically acceptable range of Γ_e and α values that cause seizures for the range of P_{ee} used here. The excitatory inputs in the first case are higher, and produce more robust seizures that require greater increases in inhibition to suppress seizures.

A. Seizures with Γ_e = 0.0008 and $\alpha = 1.6$

A temporal distribution of P_{ee} with a maximum value of 548.0 as shown in the right most panel of fig. 1 ensures a gradual increase in the mean soma potentials of both neuron populations

until the cortex is tipped into a state of seizures. The seizures produced using these values of P_{ee}, Γ_e, and α, simulate the activity of some of the most physiologically robust seizures seen in the human cortex [34]. The left most panel of figure 1 depicts the variation of the mean soma potential of the excitatory population with time, and the center panel of figure 1 represents a one dimensional slice of the two dimensional domain illustrating traveling waves when seizure like activity is observed for the range of P_{ee} shown in the right most panel of the same figure. It should be noted here that the seizure waves may appear to be almost stationary in a 1D slice of the two dimensional cortex. These are, in fact, spiral waves with large radii of curvature as illustrated in [11]. The smaller cortex used in this work has dimensions of the order of a human cortex, making it difficult to appreciate the curvature of the traveling waves, which have radii of curvature of the order of the dimensions of the model human cortex. Interestingly, while high values of P_{ee} are required to initiate seizures, lower values of P_{ee} are able to sustain seizure like activity as seen in fig. 3. Oscillatory activity seizes when the magnitude of P_{ee} falls well below 270 despite starting only after P_{ee} has risen past a value of around 300, as shown in fig. 1a.

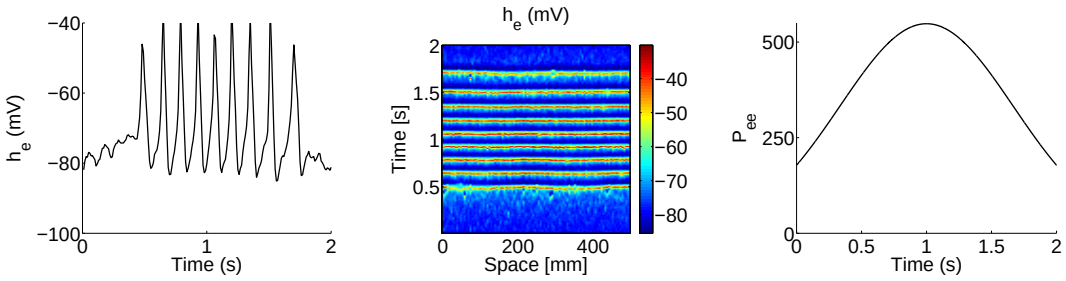

FIG. 1: Seizures in the P_{ee}-Γ_e space. P_{ee} is gradually increased then decreased in time with a maximum value of 548.0 as shown in the figure on the extreme right. Γ_e is held constant at 0.0008 with $\alpha = 1.6$. All other parameters are similar to baseline parameters in [13]. The mean soma potential ($\tilde{h}_e$) at a point, and traveling seizure waves depicted by a 1 dimensional slice of the 2 dimensional cortex are shown in the first two figures on the left.

Seizures arising with this set of parameters are successfully suppressed by using closed loop optogenetic stimulation as shown in fig.2. The intensity is calculated using eq. 8, and is triggered when $\tilde{h}_m$ surpasses a magnitude of 0.2, coupled with a 20 % change in $\tilde{h}_m$ over 20 ms. When the amplitude of measured potential $\tilde{h}_m$ and the intensity of light illuminating the model cortex fall below 0.1 and 10 mw/mm^2, respectively, control is switched off. The

proportional and integral gains for the controller are tuned to suppress a fully formed seizure at $P_{ee} = 548.0$, $\Gamma_e = 0.0008$ and $\alpha = 1.6$. An open loop intensity of 34 mW/mm^2 is required to control the same seizures. The red dot dash line in the right most panel of figure 2 depicts the intensity of open loop illumination required to suppress the same seizure. The on and off switch for the controller is based on the amplitude and rate of change thresholds used to detect seizures in section III B. Again, seizures are detected just as they begin to take shape, and control is triggered around 0.5s as seen in panel on the right in fig. 2. As the strength of subcortical inputs peaks around 1s, there is a slight increase in the illumination intensity required to subdue oscillatory activity. Intensity continues to decrease almost monotonically after this increase at 1s.

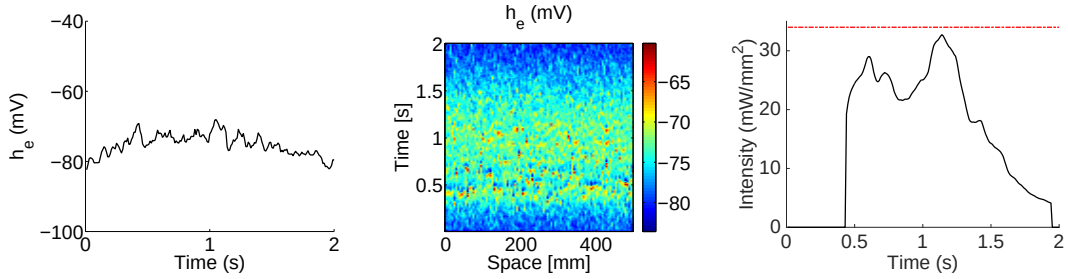

FIG. 2: Effect of closed loop optogenetic control on seizures in the P_{ee}-Γ_e space using a temporal modulation of P_{ee} in time shown in fig. 1c. Γ_e is held constant at 0.0008 with $\alpha = 1.6$. All other parameters are similar to baseline parameters in [13]. Figures on the extreme left and right show the variation with time of h_e and intensity, respectively, at the same point. The red dot-dash line in the figure on the extreme right indicates the open loop intensity required to suppress a fully formed seizures at $P_{ee} = 548.0$. Gains used: $K_P = 0.4$ and $K_I = 3.6$.

The seizure in fig. 2 is rather robust, and requires higher intensities to suppress oscillatory activity as compared to the seizures described in the next section. The controller is tuned to use optimal amounts of energy while operating within the physiological bounds for tissue exposure to light. A high proportional gain will react more vigorously to the robust changes in mean soma potential caused by the higher excitatory inputs, and might synchronise the optogenetic and cortical dynamics leading to continued oscillatory activity. Additionally, high proportional gains might lead to rapid increases in illumination intensities well past physiologically safe

values. The integral term provides the required offset to these drawbacks of purely proportional control. Higher integral gains lead to higher overall intensities, which are required to suppress robust oscillations in the model cortex.

B. Seizures with Γ_e = 0.00066 and $\alpha = 1.15$

In this section, we look at a less robust seizure with lower excitatory inputs. The seizure pathway is the same as the seizure studied in the previous subsection, however, the influence of the excitatory post synaptic potential (EPSP) denoted by Γ_e, and the amplitude of noise, α, in the stochastic subcortical inputs are both decreased. The left and center panel of figure 3 show the variation of the excitatory mean soma potential at a point and the traveling seizure waves in the model cortex, respectively. Again, the subcortical inputs from the excitatory population to itself is varied with time as shown in the right most panel of fig. 3. As observed in fig. 1, seizures start at a higher P_{ee} but are sustained even after the subcortical inputs have fallen below this initial value. However, we use a smaller range of P_{ee} values here, and this leads to two distinct differences with the seizures seen in section III A. One, for higher values of Γ_e and α seizures arise at a much lower value of P_{ee}. Two, we can clearly see the end of the seizure state in the left and center panels of figure 3, with oscillatory activity being suppressed around the 1.8 s mark, while it is less apparent in the seizures described in this section.

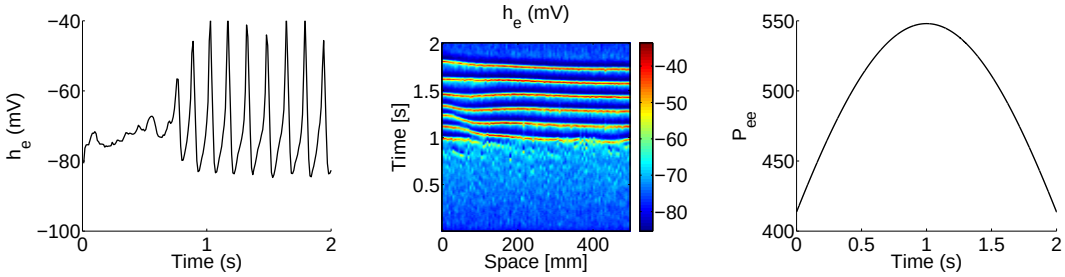

FIG. 3: Seizures in the P_{ee}-Γ_e space. P_{ee} is gradually increased then decreased in time with a maximum value of 548.0 as shown by the figure in the panel on the right. Γ_e is held constant at 0.00066 with α = 1.15. All other parameters are similar to baseline parameters in [13]. The mean soma potential ($\tilde{h}_e$) at a point, and traveling seizure waves depicted by a 1 dimensional slice of the 2 dimensional cortex are shown in the first two figures on the left.

Figure 4 shows the effect of closed loop optogenetic control on a model cortex with weak seizures. Control is actuated by depolarising the inhibitory neurons. The increased inhibition suppresses the tendency of high subcortical inputs to hyperexcite the model cortex. The controller is tuned to suppress the strongest seizures arising in the $P_{ee} - \Gamma_e$ plane, making it robust to temporal variations in parameter values. Fig. 4 clearly demonstrates the advantages of having a controller that calculates intensity based on the measured signal, as opposed to using an open loop approach. The controller outperforms the open loop controller using optimal intensity instead of a constant intensity to suppress seizures. The right most figure in fig. 4 shows that the mean soma potential is maintained around the rest potential of the excitatory population for the given values of Γ_e and P_{ee}. The central panel of fig. 4 also shows the suppression of traveling seizure waves demonstrating a breakdown of oscillatory behavior.

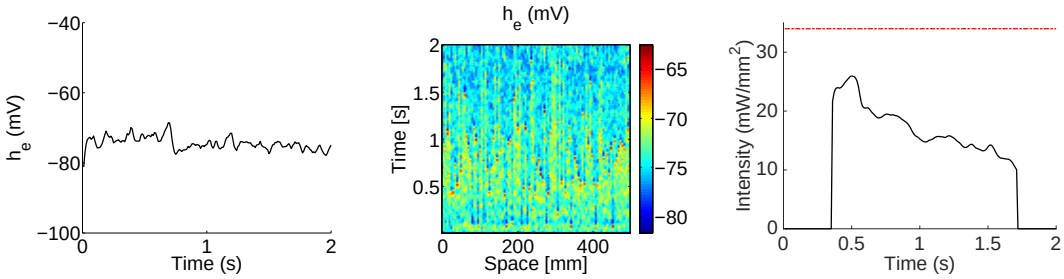

FIG. 4: Effect of closed loop optogenetic control on seizures in the P_{ee}-Γ_e space using a temporal modulation of P_{ee} in time shown in fig. 1c. Γ_e is held constant at 0.00066 with $\alpha = 1.15$. All other parameters are similar to baseline parameters in [13]. Figures on the extreme left and right show the variation with time of h_e and intensity, respectively, at the same point. The red dot-dash line in the figure on the extreme right indicates the open loop intensity required to suppress a fully formed seizures at $P_{ee} = 548.0$, $\Gamma_e = 0.0008$, and $\alpha = 1.6$. Gains used: $K_P = 0.4$ and $K_I = 3.6$, which are the same gains used to suppress the robust seizure presented in section III A.

IV. THE ODE MODEL

The stochastic and spatial terms in the set of stochastic partial differential equations (SPDEs) that describe the meso-scale cortical model make bifurcation analysis, which can provide useful

insight into the seizure dynamics of the model, a challenging task. To gain a preliminary insight into the rich dynamics of this system via bifurcation analysis, the stochastic inputs and spatial terms from the SPDEs, which can be found in Appendix A, that describe the cortical model are ignored, and a simpler ordinary differential equation (ODE) system is considered. The combined optogenetic and cortical ODE system is stated here:

$$\frac{d\tilde{h}_e}{d\tilde{t}} = 1 - \tilde{h}_e + \Gamma_e(h_e^0 - \tilde{h}_e)\tilde{I}_{ee} + \Gamma_i(h_i^0 - \tilde{h}_e)\tilde{I}_{ie} \tag{10}$$

$$\frac{d\tilde{h}_i}{d\tilde{t}} = 1 - \tilde{h}_i + \Gamma_e(h_e^0 - \tilde{h}_i)\tilde{I}_{ei} + \Gamma_i(h_i^0 - \tilde{h}_i)\tilde{I}_{ii} - u \tag{11}$$

$$\left(\frac{1}{T_e}\frac{d}{d\tilde{t}} + 1\right)^2 \tilde{I}_{ee} = N_e^\beta \tilde{S}_e\left[\tilde{h}_e\right] + \tilde{\phi}_e + P_{ee} \tag{12}$$

$$\left(\frac{1}{T_e}\frac{d}{d\tilde{t}} + 1\right)^2 \tilde{I}_{ei} = N_e^\beta \tilde{S}_e\left[\tilde{h}_e\right] + \tilde{\phi}_i + P_{ei} \tag{13}$$

$$\left(\frac{1}{T_e}\frac{d}{d\tilde{t}} + 1\right)^2 \tilde{I}_{ie} = N_i^\beta \tilde{S}_i\left[\tilde{h}_i\right] + P_{ie} \tag{14}$$

$$\left(\frac{1}{T_e}\frac{d}{d\tilde{t}} + 1\right)^2 \tilde{I}_{ii} = N_i^\beta \tilde{S}_i\left[\tilde{h}_i\right] + P_{ii} \tag{15}$$

$$\left(\frac{1}{\lambda_e}\frac{d}{d\tilde{t}} + 1\right) \tilde{\phi}_e = N_e^\alpha \tilde{S}_e\left[\tilde{h}_e\right] \tag{16}$$

$$\left(\frac{1}{\lambda_i}\frac{d}{d\tilde{t}} + 1\right) \tilde{\phi}_i = N_i^\alpha \tilde{S}_e\left[\tilde{h}_e\right] \tag{17}$$

$$\frac{dN_{O1}}{d\tilde{t}} = K_{a1}.N_{C1} - (K_{d1} + e_{12}).N_{O1} + e_{21}.N_{O2} \tag{18}$$

$$\frac{dN_{O2}}{d\tilde{t}} = K_{a2}.N_{C2} + e_{12}.N_{O1} - (K_{d2} + e_{21}).N_{O2} \tag{19}$$

$$\frac{dN_{C2}}{d\tilde{t}} = K_{d2}.N_{O2} - (K_{a2} + K_r).N_{C2}, \tag{20}$$

Eqs. 10-17 represent the cortical model and eqs. 18-20 describe the dynamics of ChR2 optogenetic channels. This system has been recast in dimensionless variables and all variables are functions of dimensionless time $\tilde{t}$ only. The subscripts e and i represent excitatory and inhibitory populations respectively, and variables with two subscripts in the cortical model represent the transfer of energy from one population to another. The mean soma potential of each population is denoted by $\tilde{h}$, post-synaptic connections by $\tilde{I}$, and long range connections by $\tilde{\phi}$. N represents the fraction of ChR2 channels in each of the four states, while K is the rate of transition from one state to another as described in [11]. Again, tildes represent non-dimensionalized variables in the cortical model. The control term u is given by,

$$u = \tilde{h}_i.G_{ChR2}.R_m. \tag{21}$$

In equation 21, $\tilde{h}_i$ is the mean soma potential of the inhibitory population, G_{ChR2} is the channel conductivity described in equation 5, and the membrane resistance R_m is obtained from voltage clamp experiments and has a value of $7.1G\Omega$[8]. **Various studies have shown the reversal potential of ChR2 channels at physiological PH is 0 mV [41, 46–48]. The PH around a cortical macrocolumn will not be affected significantly under optogenetic stimulation, so we assume a reversal potential of 0 mV for the optogenetic model.** The values of all constants connected to the cortical model can be found in [10] and values of rate constants associated with the optogenetic model can be referenced in [11]. We use AUTO [35], a software package for continuation and bifurcation problems in ordinary differential equations, to study this system of equations and to determine the associated fixed points, bifurcations, limit cycles and their stability type. Please see [36] for a specific implementation of bifurcation analysis of the meso-scale cortical model with spatial and temporal variation but without stochastic inputs.

The figure on the left in fig. 5 shows the comparison between the SPDE and ODE models for a hyperexcited model cortex with subcortical input $P_{ee} = 548.0$. Red represents the maximum and minimum values of h_e over 2 seconds for a given Γ_e using the SPDE model while black represents the bifurcation diagram of the ODE model. In figure 5a, the amplitude of noise from the stochastic subcortical inputs, defined in Appendix A, is set at 0.1 to demonstrate the effect of the spatial terms on the SPDE model, and how the dynamics compare to the ODE model. This is an order of magnitude lower than the amplitude used in other simulations presented in this paper using the SPDE model where $\alpha = 1.15$ or 1.6. Apart from high amplitude oscillations occurring at a lower Γ_e using the SPDE model, the dynamics of the SPDE model follow that of the ODE model closely in stable regions (solid lines). This agreement between the SPDE and ODE models makes it reasonable to use the simpler ODE model to perform a dynamical systems analysis on the cortical model, which may be suggestive of what happens in the full SPDE model. The right panel of fig. 5 shows the region of P_{ee}-Γ_e space that leads to oscillatory behaviour in the ODE and SPDE models denoted by dark grey and light grey regions, respectively. In this figure, $\alpha = 1.6$ is used to account for the full effect of noise in the SPDE

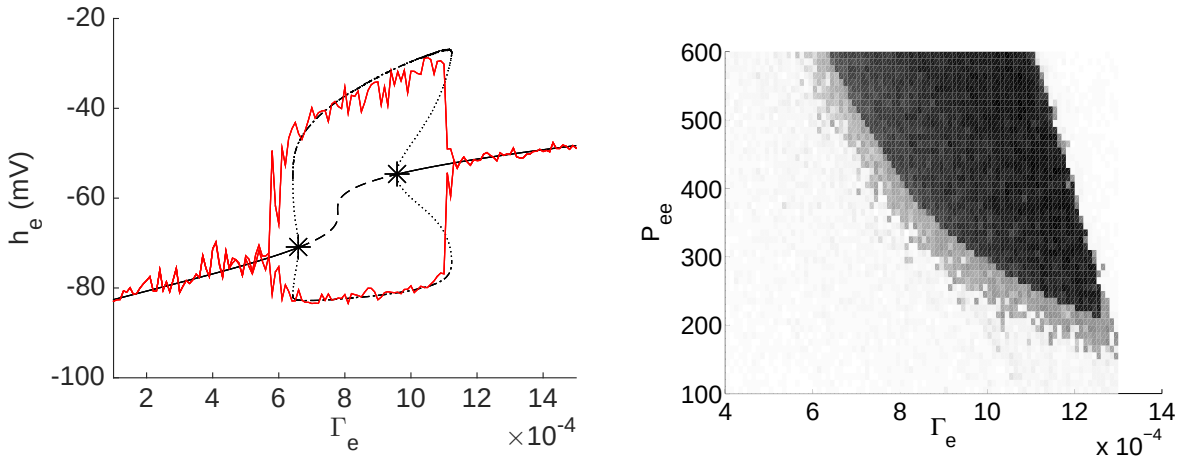

FIG. 5: Comparison between the full SPDE model and the simpler ODE model. **Left:** Response diagram for the hyperexcited cortex with subcortical input $P_{ee} = 548.0$. Amplitude of noise from stochastic subcortical inputs was reduced by an order of magnitude to 0.1 to demonstrate the effect of spatial terms on the dynamics of the model. The red jagged lines indicate maximum and minimum values of h_e over 2 seconds for different Γ_e, which is the influence of the synaptic input on the mean soma potential of the excitatory population, using the SPDE model. Black lines indicate the bifurcation diagram for the ODE model. Dashed and solid lines indicate unstable and stable fixed points, respectively. Maximum and minimum values of h_e during stable (dot-dashed) and unstable (dashed) limit cycles arising from a subcritical Hopf bifurcation (asterisk) are also shown. **Right:** Comparison of the SPDE and ODE models in parameter space, with grey regions indicating seizure causing areas. The stochastic inputs in the SPDE model enhance the seizure area (indistinct boundary marked in grey) in parameter space when compared to the ODE model (darker region with sharp boundaries). Here, we use $\alpha = 1.6$ which corresponds to the amplitude of noise used with the SPDE model elsewhere in the manuscript.

model. Except at the boundaries, the seizure causing region using the ODE model overlaps that of the SPDE model almost entirely. The SPDE model has boundaries for the seizure regions that are slightly broader and less distinct than the boundaries of the ODE model.

A. Bifurcation analysis using the ODE system

In section III, P_{ee} was gradually varied until a high enough magnitude of excitatory subcortical inputs induced seizures in the model cortex. Here, we study the response of the cortical model by observing the features of the mean soma potential of the excitatory population when the magnitude of excitatory subcortical inputs is varied. The left most panel of fig. 6 shows the response of the ODE model when no optogenetic stimulation is applied at $\Gamma_e = 0.0008$ with all other parameters held at baseline values [13]. Asterisks at $P_{ee} = 417.4$ and $P_{ee} = 996.7$ indicate subcritical Hopf bifurcations that give rise to unstable limit cycles, which stabilise at the turning points on the branch. Maximum and minimum values of h_e achieved during stable and unstable limit cycles are indicated by dot-dashed lines and dotted lines, respectively. We do not explore the dynamics past $P_{ee} = 2000.0$, which is well above the physiological limit of P_{ee}. Stable oscillations (dot-dashed lines) occur between $P_{ee} = 397.2$ and $P_{ee} = 1355.0$.

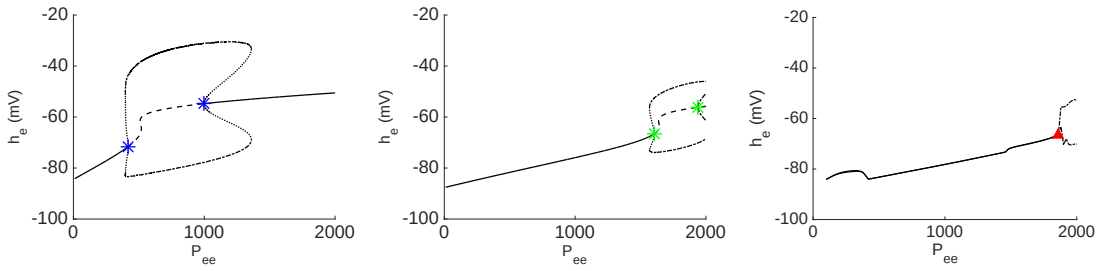

FIG. 6: Bifurcation analysis using an unstimulated cortex (left panel) and a cortex stimulated with light of constant 10 mW/mm^2 intensity in the open loop configuration (center panel). Asterisks indicate subcritical Hopf bifurcations that lead to unstable limit cycles. Time integration of the combined cortico optogenetic model with PI control to track the maximum and minimum values of the excitatory mean soma potential is shown on the right. The red triangle indicates the start of oscillatory activity despite closed loop control being triggered. The dashed black lines in the right most panel indicate minimum and maximum values of $\tilde{h}_e$ during oscillatory activity arising despite the use of closed loop control. Gains used $K_P = 0.4$ and $K_I = 3.6$.

To evaluate the efficacy of open loop optogenetic control, we use an intensity of 34 mW/mm^2, which is the minimum intensity required to suppress successfully a fully formed

seizure when $\alpha = 1.6$, $\Gamma_e = 0.0008$, and P_{ee} is within the physiologically acceptable range of values. When open loop optogenetic control is applied via the inhibitory population using an illumination intensity of 34 mW/mm^2 the first and second subcritical Hopf bifurcations, marked with green asterisks, shift to higher values of $P_{ee} = 1604.67$ and $P_{ee} = 1938.87$, respectively. These Hopf bifurcations also lead to an unstable limit cycle, and demonstrate how open loop can delay seizure activity until much higher excitatory inputs are available to elicit seizures.

In the case with triggered PI control, we cannot perform a bifurcation analysis because the trigger renders the system discontinuous in time. Instead, we time integrate the ODE system to obtain the maximum and minimum values of the mean soma potential for various values of P_{ee}, as shown in the right most panel of 6. After control is triggered, we simulate cortical activity for a further 1 second. This is done to allow the system to reach a steady state, which in turn allows us to track the maximum and minimum value of the mean soma potential for the excitatory population after the control effort has attained maximum strength. The black solid line indicates no oscillatory activity in the cortex when control is switched on (stable fixed points), while the black dot dashed lines indicate oscillations in the mean soma potential of the excitatory population despite control being turned on. The red triangle around $P_{ee} = 1860.0$ indicates the lowest value of subcortical excitatory inputs that will produce seizures in the ODE model despite the use of closed loop optogenetic control. Here, we use $K_P = 0.4$ and $K_I = 3.6$. In both the open and closed loop cases, we do not explore higher intensities or gains because they successfully delay oscillatory activity well past the physiological range of parameters.

V. SEIZURES IN THE M_e-Γ_i SPACE

Another route to seizure using the meso scale cortical model is achieved by increasing the slope at the inflection point of the sigmoid function that represents the mean firing rate of the excitatory population, M_e, as it depends upon the mean soma potential of the excitatory population, $\tilde{h}_e$. This parameter models the effects of variance of depolarisation within a population of neurons [37]. By increasing M_e, small changes in $\tilde{h}_e$ could result in large changes in the firing rate $\tilde{S}_e$, a characteristic of oscillatory behavior. When Γ_i, the influence of synaptic input on mean soma potential, is also increased by a small amount, it leads to a small net increase in the rate of change of $\tilde{h}_e$. This rise in $d\tilde{h}_e/d\tilde{t}$ coupled with the higher M_e leads to an abrupt onset of oscillatory behavior as observed in figure 7. We gradually increase, and then decrease, M_e in

time as shown in the right most panel of figure 7, while Γ_i is held at a slightly higher values than during normal function. The value of M_e at its peak is -12.5, which is within the physiological range of values for this parameter, but is much higher than its value during normal function.

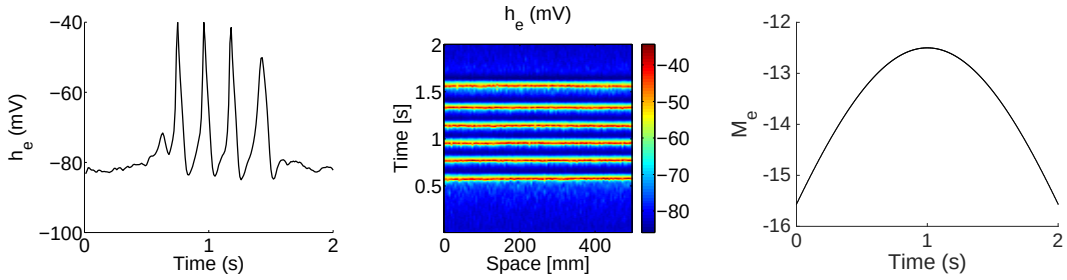

FIG. 7: Seizures in the M_e-Γ_i space using a variation of M_e in time with a maximum value of -12.5 as shown in the panel on the right. Γ_i is held constant at 0.085. All other parameters are similar to baseline parameters in [13]. The mean soma potential ($\tilde{h}_e$) at a point, and traveling seizure waves depicted by a 1 dimensional slice of the 2 dimensional cortex are shown in the first two figures on the left.

The center panel of figure 7 depicts a one dimensional slice of the 2D domain illustrating traveling waves. The waves appear to be stationary because the radius of curvature of spiral waves produced is much larger than the dimensions of the model. When seizures are induced by increasing subcortical inputs and decreasing the influence of excitatory synapses on the mean soma potential, there is first a gradual increase in the post synaptic activation, which results in an increase in the firing rate that leads to highly oscillatory activity. However, when we change Γ_i and M_e, we directly increase the firing rate. This leads to a more abrupt onset seizure. Consequently, seizure like activity is quickly suppressed when M_e is reduced.

To deal with the abruptness of seizure onset by quickly suppressing excessive excitatory activity, a strong initial control effort is required. This is achieved by using a relatively high proportional gain, $K_P = 1.0$, and a moderately high integral gain, $K_I = 0.64$. A higher intensity leads to higher optogenetic conductance, which in turn depolarises inhibtory cells much faster. The gains are tuned for a fully formed seizure with parameters $M_e = -12.5$, $\Gamma_i = 0.085$ and $\alpha = 1.6$. An open loop intensity of 8 mW/mm^2 is required to suppress an equivalent fully formed seizure. The red dot-dash lines in figure 8c depicts open loop intensity for fully formed seizures at the peak value of $M_e = -12.5$. The intensities used to suppress seizures in this space

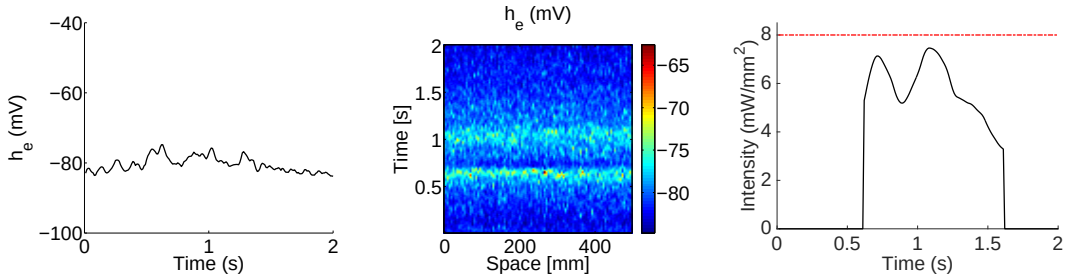

FIG. 8: Effect of closed loop optogenetic control on seizures in the M_e-Γ_i space. M_e is varied in time with a maximum value of -12.5 as shown in figure 7. Γ_i is held constant at 0.085 with $\alpha = 1.6$. All other parameters are similar to baseline parameters in [13]. The left and right panels show the variation with time of $\tilde{h}_e$ and intensity, respectively at the same point. The red dot-dash line in the right panel indicates the open loop intensity required to suppress a fully formed seizures at $g_e = -12.5$. Gains used: $K_P = 1.0$ and $K_I = 0.64$.

are lower than intensities observed in III A because unlike constant high subcortical inputs, a high M_e leads to rapid oscillations between high and low firing rates, which translates to the amplitude of total excitatory inputs in the model cortex oscillating between highs and lows. This gives the increased inhibition from optogenetic stimulation more opportunities for seizure suppression using lower intensities when the firing rate is low.

The delays associated with synaptic transmission make the rapidity in depolarisation crucial to suppressing excessive excitatory activity before it reaches a state of synchronisation characteristic of seizures. As M_e rises until it peaks at 1s, the firing rate increases and decreases more rapidly, and the controller accounts for these changes by adjusting the intensity of light as seen in the panel on the right in figure 8. We have used the same amplitude and rate triggers as in the previous section. The left and center panels of figure 8 respectively show how oscillations in h_e are suppressed, and how traveling seizure waves break down.

A. Seizures in parameter space

Figure 9 illustrates the region of the M_e-Γ_i space that leads to seizure like activity in the model cortex. Open loop control via an 8 mW/mm^2 illumination and closed loop PI control with K_P = 1.0 and K_I = 0.64 successfully suppress oscillatory activity throughout the entire

range of values of M_e and Γ_i shown in figure 9, and so we have not shown this parameter space or the bifurcation diagram here with illumination turned on. Again, the SPDE model will lead to less distinct boundaries of the seizure area in parameter space.

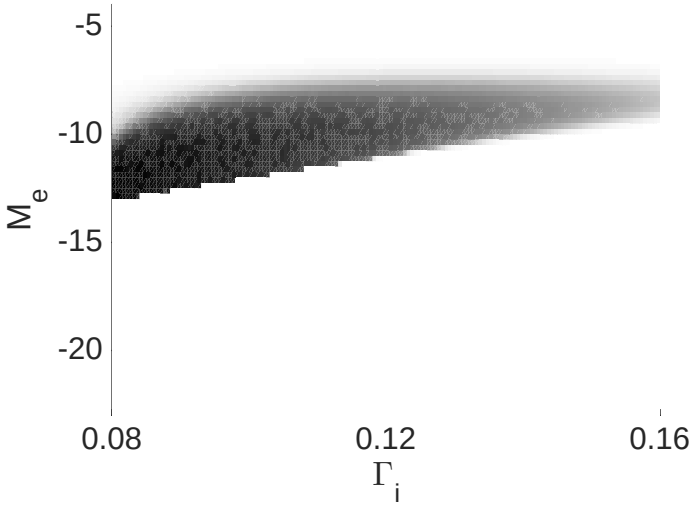

FIG. 9: Seizure prone areas in the $M_e - \Gamma_i$ parameter space with no optogenetic stimulation. Here, dark regions represent values of M_e and Γ_i which produce oscillations in the mean soma potential h_e. The grayscale shading indicates the variation in h_e during oscillatory behavior. These results were obtained using the dimensionless ODE system of equations.

VI. CONCLUSION

We have presented a method of closed loop optogenetic control that efficiently suppresses seizure like activity in a model of the human cortex. The inhibitory population in the cortical model is modified to express channelrhodopsin-2 (ChR2) ion channels that are activated by light of wavelength 480 nm. A simple and robust trigger initiates control when seizure like activity is detected via amplitude and rate of change of amplitude thresholds of electrode measurements of cortical activity ($\tilde{h}_m$), which are made at the same temporal and spatial scales that define the cortical model. Proportional integral (PI) control based on the measured potential is used to calculate the intensity of light that illuminates the inhibitory population together with an algorithm for switching off the controller when the seizure subsides. Depolarising the inhibitory population increases inhibition, which in turn suppresses excessive excitatory activity characteristic of epileptic seizures. This control strategy is tested in the P_{ee}-Γ_e and $M_e - \Gamma_i$ parameter spaces,

which have been found to be the most probable parameter regions that lead to seizures in the model that correspond well with multiple seizures observed in recordings of cortical activity of a patient [34]. Bifurcation analysis in the P_{ee}-Γ_e space reveals that even a small intensity of light delays the occurrence of Hopf bifurcations that lead to unstable limit cycles, which signal seizure like activity in the model cortex. The etiology of seizures is important in determining the gain constants associated with control. Abrupt onset of seizures, as seen in the $M_e - \Gamma_i$ parameter space require a higher proportional response. A more gradual increase in oscillatory activity, as seen in the P_{ee}-Γ_e, requires lower intensities of light illumination to inhibit seizure activity. An examination of a simpler ODE model that corresponds well with the full SPDE model, shows the effectiveness of closed loop control in suppressing physiologically relevant seizures in the model cortex.

While this strategy of seizure control is effective, there are improvements that can be made. First, we can account for the spatial electrode profile in our measurements to improve the accuracy of the measured potential, and also incorporate spatial variation of illumination that could result in less homogeneous distribution of intensity. We can also account for spatial variations of the cortical model, for example the presence of gyri and sulci, making only a region of model cortex easily accessible to optogenetic stimulation. In [11] we showed optogenetic control is still effective when only parts of the cortical model are illuminated. However, a limited region of stimulation might require higher illumination intensities, and a more refined tuning of the gain terms.

Second, as stated in section II B, different types of inhibitory neurons could be responsible for specific types of seizures. Previous work [11], has explored the consequences of stimulating only a fraction of the neurons in the meso-scale model to inhibit seizure activity. Using constant illumination, control was achieved when only a third of the inhibitory population in the area of a seizure hotspot was stimulated with higher illumination intensities. It would be interesting to investigate how stimulation via different neuron subtypes influences the dynamics of seizures in the human cortex. While we currently do not have sufficient data on different types of human interneurons to include them in our model, in rats [43, 44] and in mice [45], inhibitory neurons can be divided into three main subtypes, fast spiking, latent spiking and another group containing burst spiking and regular spiking neurons. The meso-scale model offers a very suitable platform to incorporate the dynamics of these neurons because the layout of the equations of the model facilitates the inclusion of more sub-types of neurons.

Third, we have seen seizures can be more abrupt in the $M_e - \Gamma_i$ parameter space, which suggests exploring control actuation via the excitatory population to mitigate the effect of synaptic delays by suppressing excessive excitation at the source. One way of doing this is to use halorhodpsin, which is an anion pump that is activated by light of wavelength around 570 nm [38], to hyperpolarise the excitatory neurons. Apart from avoiding synaptic delays, another advantage of using this method in conjunction with our current method of control is the option of selectively stimulating either inhibitory or excitatory neurons, or stimulating both together to provide more flexible control.

Finally, it will be interesting to study the effects of optogenetic stimulation of subcortical brain structures. Some seizures specifically arise because of the dynamic interplay between the cortex and subcortical regions. For example, in [21], seizures arising from cortical injury, and maintained by the interplay between the thalamus and cortical regions were identified in rats. Additionally, in the same paper, thalamocortical neurons were stimulated via closed loop optogenetic control to inhibit seizures caused by cortical injury. The meso-scale mathematical model of the cortex used in this work does not yet include detailed equations describing the dynamic interplay between subcortical and cortical regions, which may only be a feature in some seizures. Instead, we explore whether seizures caused by higher excitatory subcortical inputs or changes in the inflection point of the sigmoid function that describes the mean excitatory firing rate could be controlled with optogenetics in the cortex, which is a much more accessible part of the brain to stimulate than subcortical regions. The control of specific seizures might entail other, more involved strategies. This first attempt at exploring whether cortical feedback stimulation could work has proven successful even when the precipitating cause is subcortical inputs. In the future, a complex mathematical model of dynamic cortico-subcortical interactions, will aid in studying the effect of applying optogenetic control to subcortical regions, and also provide insight into the effects of cortical stimulation when the pathway to seizures is the dynamic interplay between the cortex and subcortical regions.

ACKNOWLEDGMENT

This work was partially supported by the US National Science Foundation (NSF) grant CMMI 1031811.

Appendix A: The meso-scale cortical model

The non-dimensional meso-scale model was first stated in [13], where values and explanations for all variables and constants of the model can be found. For convenience, we state the equations here.

$$\frac{\partial \tilde{h}_e}{\partial \tilde{t}} = 1 - \tilde{h}_e + \Gamma_e(h_e^0 - \tilde{h}_e)\tilde{I}_{ee} + \Gamma_i(h_i^0 - \tilde{h}_e)\tilde{I}_{ie} \tag{A1}$$

$$\frac{\partial \tilde{h}_i}{\partial \tilde{t}} = 1 - \tilde{h}_i + \Gamma_e(h_e^0 - \tilde{h}_i)\tilde{I}_{ei} + \Gamma_i(h_i^0 - \tilde{h}_i)\tilde{I}_{ii} \tag{A2}$$

$$\left(\frac{1}{T_e}\frac{\partial}{\partial \tilde{t}} + 1\right)^2 \tilde{I}_{ee} = N_e^\beta \tilde{S}_e\left[\tilde{h}_e\right] + \tilde{\phi}_e + P_{ee} + \tilde{\Gamma}_1 \tag{A3}$$

$$\left(\frac{1}{T_e}\frac{\partial}{\partial \tilde{t}} + 1\right)^2 \tilde{I}_{ei} = N_e^\beta \tilde{S}_e\left[\tilde{h}_e\right] + \tilde{\phi}_i + P_{ei} + \tilde{\Gamma}_2 \tag{A4}$$

$$\left(\frac{1}{T_i}\frac{\partial}{\partial \tilde{t}} + 1\right)^2 \tilde{I}_{ie} = N_i^\beta \tilde{S}_i\left[\tilde{h}_i\right] + P_{ie} + \tilde{\Gamma}_3 \tag{A5}$$

$$\left(\frac{1}{T_i}\frac{\partial}{\partial \tilde{t}} + 1\right)^2 \tilde{I}_{ii} = N_i^\beta \tilde{S}_i\left[\tilde{h}_i\right] + P_{ii} + \tilde{\Gamma}_4 \tag{A6}$$

$$\left(\frac{1}{\lambda_e}\frac{\partial}{\partial \tilde{t}} + 1\right)^2 \tilde{\phi}_e = \frac{1}{\lambda_e^2}\nabla^2\tilde{\phi}_e + \left(\frac{1}{\lambda_e}\frac{\partial}{\partial \tilde{t}} + 1\right) N_e^\alpha \tilde{S}_e\left[\tilde{h}_e\right] \tag{A7}$$

$$\left(\frac{1}{\lambda_i}\frac{\partial}{\partial \tilde{t}} + 1\right)^2 \tilde{\phi}_i = \frac{1}{\lambda_i^2}\nabla^2\tilde{\phi}_i + \left(\frac{1}{\lambda_i}\frac{\partial}{\partial \tilde{t}} + 1\right) N_i^\alpha \tilde{S}_e\left[\tilde{h}_e\right] \tag{A8}$$

All variables have been non dimensionalized and are functions of time $\tilde{t}$, and the two spatial dimensions $\tilde{x}$ and $\tilde{y}$. The subscripts e and i represent excitatory and inhibitory populations respectively, and variables with two subscripts represent the transfer of energy from one population to another. Tildes over parameters and parameters represented by upper case letters indicate non-dimensionalized forms. The mean soma potential for a neuronal population is represented by the $\tilde{h}$ state variable, $\tilde{I}$ represents the postsynaptic activation due to local, long-range, and subcortical inputs. $\tilde{\phi}$ represents long range (corticocortical) inputs. The stochastic forcing from the subcortical inputs is represented by $\tilde{\Gamma}_{1,2,3,4}$ terms in equations A3 - A6. In equations A7 and A8, ∇^2 represents the Laplacian, or the divergence of the gradient of the long rang connections ϕ, which models the spatial variation of the long range connections. The stochastic forcing and spatial terms can be removed to obtain the ODE model described in section IV.

The firing rate of each neuron population is given by the sigmoid function $\tilde{S}_{e,i}$, and is dependent on the mean soma potential of the population, $\tilde{h}_{e,i}$, the inflection point of the sigmoid

function, $\tilde{\theta}_{e,i}$, and the slope at the inflection point of the sigmoid function, $M_{e,i}$. **Please note that $M_{e,i}$ in this article corresponds to $\tilde{g}_{e,i}$ in Kramer et al. [13]. We have changed notation to avoid confusion with the various conductance variables associated with the optogenetic model that are denoted by g.**

$$\tilde{S}_{e,i} = \frac{1}{1 + exp[-M_{e,i}(\tilde{h}_{e,i} - \tilde{\theta}_{e,i})]} \tag{A9}$$

Subcortical inputs contribute to the postsynaptic activation I_{ij} through constant P_{ij} and stochastic inputs defined by,

$$\tilde{\Gamma} = \alpha \sqrt{P_{ij}} \xi [\tilde{x}, \tilde{t}]. \tag{A10}$$

Here, i and j refer to population subtypes, which can be either excitatory or inhibitory, α is a scaling parameter for the stochastic inputs ξ is zero mean Gaussian white noise in time and space.

For convenience, we include tables from [13] that explain the dimensionless variables in terms of the dimensional symbols (Table 1), and the associated parameters and their typical values (Table 2).

Symbol	Definition	Description
$\tilde{h}_{e,i}$	$h_{e,i}/h^{rest}$	Population mean soma dimensionless electric potential
$\tilde{I}_{ee,ie}$	$I_{ee,ie}\gamma_e/G_e exp(1)S^{max}$	Total $e \to e, i \to e$ input to excitatory population
$\tilde{I}_{ei,ii}$	$I_{ei,ii}\gamma_i/G_e exp(1)S^{max}$	Total $e \to i, i \to i$ input to inhibitory population
$\tilde{\phi}_{e,i}$	$\phi_{e,i}/S^{max}$	Long range (corticortical) input to e, i populations
t	t/τ	Dimensionless time
x	$x/(\tau\tilde{v})$	Dimensionless time

TABLE I: Dynamical variable definitions for the dimensionless SPDEs model. The dimensionless variables (left column) are defined in terms of the dimensional symbols (middle column) found in Table 1 (with values and description) of Steyn-Ross et al. [6]. The variables are described in the right column. Subscripts e and i refer to excitatory and inhibitory populations, respectively. The notational simplification is made in agreement with values used in [6].

Appendix B: The optogenetic model

For convenience, we include a table explaining the rate constants in eqs.1-3 that appears in Selvaraj et al. [11].

The photon flux is dependent on the light intensity E:

$$\phi = \frac{\sigma E \lambda}{hc}, \tag{B1}$$

where ϕ is the photon flux at a given time, σ is the effective cross section of a ChR2 channel ($\sim 10^{-20} m^2$), E is the intensity of light in W/m^2, λ is the wavelength of light used (blue light - 470 nm), h is Planck's constant, and c is the speed of light.

Symbol	Definition	Description	Typical value
$\Gamma_{e,i}$	$\frac{G_{e,i}exp(1)S^{max}}{\gamma_{e,i}\lvert h^{rev}_{e,i}-h^{rest}\rvert}$	Influence of input on mean soma potential values	1.42×10^{-3}, 0.0774
$h^0_{e,i}$	$h^{rev}_{e,i}/h^{rest}$	Dimensionless cell reversal potential	-0.643, 1.29
$T_{e,i}$	$\tau\gamma_{e,i}$	Dimensionless neurotransmitter rate constant	12.0, 2.6
$\lambda_{e,i}$	$\tau\tilde{v}\Lambda_{ee,ei}$	Dimensionless characteristic corticocortical inverse-length scale	11.2, 18.2
$P_{ee,ie}$	$p_{ee,ie}/S^{max}$	Subcortical input to e population	11.0, 16.0
$P_{ei,ii}$	$p_{ee,ei}/S^{max}$	Subcortical input to i population	16.0, 11.0
$N^{alpha}_{e,i}$	-	Total number of synaptic connections from distant e populations	4000, 2000
$N^{beta}_{e,i}$	-	Total number of local e and i synaptic connections	3034, 536
$M_{e,i}$	$g_{e,i}/h^{rest}$	Dimensionless sigmoid slope at inflection point	-19.6, -9.8
$\tilde{\theta}_{e,i}$	$\theta_{e,i}/h^{rest}$	Dimensionless inflection point for sigmoid function	0.857, 0.857

TABLE II: Parameter values for the dimensionless SPDEs neural macrocolumn model. The dimensionless symbols (first column) are defined in terms of the dimensional variables (second column) found in Table 1 of Steyn-Ross et al. [6]. The variables are described in the third column and typical values are shown in the fourth column. The variables are described in the right column. Subscripts e and i refer to excitatory and inhibitory populations, respectively. The notational simplification is made in agreement with values used in [6].

Rate constant	Transition from	Value (ms^{-1})
K_{a1},K_{a2}	C1 to O1, C2 to O2	0.5Φ, 0.12Φ
K_{d1},K_{d2}	O1 to C1, O2 to C2	0.1, 0.5
e_{12},e_{21}	O1 to O2, O2 to O1	$.011+.005log(\Phi/0.024)$, $0.008+0.004log(\Phi/0.024)$
K_r	C2 to C1	$1/3000$

TABLE III: Rate constant values for the meso scale optogenetic model of ChR2 embedded in the cortex. $\Phi(t)$ is the photon flux per ChR2 and has units of ms^{-1}. K_{ai} is given by the quantum efficiency times the photon flux, $\varepsilon_i.\Phi(t)$.

[1] Fisher, R.S., van Emde Boas, W., Blume, W., Elger, C., Genton, P., Lee, P., Engel, J. 2005 Epileptic seizures and epilepsy: Definitions proposed by the International League Against Epilepsy (ILAE) and the International Bureau for Epilepsy (IBE). *Epilepsia* **46(4)**, 470-472.

[2] Nordli, D.R. 2005 Idiopathic generalized epilepsies recognized by the international league of against epilepsy. *Epilepsia* **46(9)**, 48-56.

[3] Liley, D.T.J., Cadusch, P.J., Dafilis, M.P. 2001 A spatially continuous mean field theory of electrocortical activity. *Network-Comp. Neural* **13**, 67-113.

[4] Lopour, B.A., Tasoglu, S., Kirsch, H.E., Sleigh, J.W., Szeri, A.J. 2011 A continuous mapping of sleep states through association of EEG with a mesoscale cortical model. *J. Comput. Neurosci.* **30**, 470-481.

[5] Dadok, V., Kirsch, H.E., Sleigh, J.W., Lopour, B.A., Szeri, A.J. 2013 A probabilistic framework for a physiological representation of dynamically evolving sleep state. *J. Comput. Neurosci.* (DOI: 10.1007/s10827-013-0489-x).

[6] Steyn-Ross, M.L., Steyn-Ross, D.A., Sleigh, J.W., Whiting, D.R. 2003 Theoretical predictions for spatial covariance of the electroencephalographic signal during the anesthetic-induced phase transition: Increased correlation length and emergence of spatial self-organization. *Phys. Rev. E* **68**, 021902.

[7] Steyn-Ross, D.A., Steyn-Ross, M.L., Sleigh, J.W., Wilson, M.T., Gillies, I.P., Wright, J.J. 2005 The sleep cycle modelled as a cortical phase transition. *J. Biol. Phys.* **31**, 547-569.

[8] Steyn-Ross, M.L., Steyn-Ross, D.A., Wilson, M.T., Sleigh, J.W.: Gap junctions mediate large-scale turing structures in a mean-field cortex driven by subcortical noise. Physical Review E **76**, 011,916 (2007)

[9] Bojak, I., Liley, D.T.J. 2005 Modeling the effects of anesthesia on the electroencephalogram. *Phys. Rev. E* **71**, 041902.

[10] Kramer, M., Kirsch, H., Szeri, A.J. 2005 Pathological pattern formation and cortical propagation of epileptic seizures. *J. R. Soc. Interface* **2**, 113-127.

[11] Selvaraj, P., Sleigh, J.W., Freeman, W.J., Kirsch, H.A., Szeri, A.J. 2014 Open loop optogenetic control of simulated cortical epileptiform activity. *J. Comput. Neurosci.* **36(3)**, 515-525.

[12] Selvaraj, P., Sleigh, J.W., Kirsch, H.A., Szeri, A.J. 2015 Optogenetic induced epileptiform activity

in a model human cortex. *Springerplus* **4**, 155.

[13] Kramer, M., Szeri, A., Sleigh, J., Kirsch, H. 2007 Mechanisms of seizure propagation in a cortical model. *J. Comput. Neurosci.* **22(1)**, 63-80.

[14] Lopour, B.A., Szeri, A.J. 2010 A model of feedback control for the charge-balanced suppression of epileptic seizures. *J. Comput. Neurosci.* **28**, 375-387.

[15] Richardson, K., Schiff, S., Gluckman, B. 2005 Control of traveling waves in mammalian cortex. *Phys. Rev. Lett*. **94(2)**, 028103.

[16] Gluckman, B., Nguyen, H., Weinstein, S., Schiff, S. 2001 Adaptive electric field control of epileptic seizures. *J. Neurosci.* **21(2)**, 590-600

[17] Yizhar, O., Fenno, L.E., Davidson, T.J., Mogri, M., Deisseroth, K. 2011 Optogenetics in neural systems. *Neuron* **71(1)**, 9-34.

[18] Grossman, N., Nikolic, K., Toumazou, C., Degenaar, P. 2011 Modeling study of the light stimulation of a neuron cell with channelrhodopsin-2 mutants. *IEEE T Biomed. Eng.* **58(6)**, 1742-1751.

[19] Bamann, C., Kirsch, T., Nagel, G., Bamberg, E. 2008 Spectral characteristics of the photocycle of channelrhodopsin-2 and its implication for channel function. *J. Mol. Biol.* **375(3)**, 686-694.

[20] Tønnesen, J., Sørensen, A., Deisseroth, K., Lundberg, C., Kokaia, M. 2009 Optogenetic control of epileptiform activity. *P. Natl. Acad. Sci. USA* **106**, 12,162-12,167.

[21] Paz, T.P., Davidson, T.J., Frechette, E.S., Delord, B., Parada, I., Peng, K., Deisseroth, K., Huguenard, J.R. 2013 Closed-loop optogenetic control of thalamus as a tool for interrupting seizures after cortical injury. *Nat. Neurosci.* **16**, 64-70.

[22] Krook-Magnuson, E., Armstrong, C., Oijala, M., Soltesz, I. 2013 On-demand optogenetic control of spontaneous seizures in temporal lobe epilepsy. *Nat. Commun.* **4:1376**, 1-8.

[23] Cardin, J., Carlén, M., Meletis, K., Knoblich, U., Zhang, F., Deisseroth, K., Tsai, L.H., Moore, C. 2010 Targeted optogenetic stimulation and recordings of neurons *in vivo* using cell type specific expression of channelrhodopsin-2. *Nat. Protoc.* **5(2)**, 247-254.

[24] Nunez, P.L., Srinivasan, R. 2006 *Electric fields of the brain: The neurophysics of EEG.* 2nd Edition, New York: Oxford University Press.

[25] Orosco, L., Laciar, E., Correa, A.G., Torres, A., Graffigna, J.P. 2009 An epileptic seizures detection algorithm based on the empirical mode decomposition of EEG. In *Conf. Proc. IEEE Eng. Med. Biol. Soc. 2009*, 2651-4.

[26] Nigam, V.P., Graupe, D. 2004 A neural-network-based detection of epilepsy. *Neurol. Res.* **26(1)**,

55-60

[27] Kannathal, N., Choo, M. L., Acharya, U.R., Sadasivan, P.K. 2005 Entropies for detection of epilepsy in EEG. *Comput. Meth. Prog. Bio.* **80(3)**, 187-194.

[28] Kumar, Y., Dewal, M. L., Anand, R. S. 2012 Epileptic seizures detection in EEG using DWT-based ApEn and artificial neural network. *Signal, Image and Video Processing* (DOI: 10.1007/s11760-012-0362-9).

[29] Jouny, C.C., Franaszczuk, P.J., Bergey, G.K. 2011 Improving early seizure detection. *Epilepsy Behav.* **22(Suppl. 1)**: S44-S48.

[30] Iasemidis, L.D., Pardalos, P., Sackellares, J.C., Shiau, D.S. 2011 Quadratic binary programming and dynamical system approach to determine the predictability of epileptic seizures. *J. Comb. Optim.* **5(1)**, 9-26.

[31] Litt, B., Esteller, R., Echauz, J., D'Alessandro, M., Shor, R., Henry, T., Pennell, P., Epstein, C., Bakay, R., Dichter, M., Vachtsevanos, G. 2001 Epileptic seizures may begin hours in advance of clinical onset: a report of five patients. *Neuron* **30(1)**, 51-64.

[32] Mormann, F., Kreuz, T., Andrzejak, R.G., David, P., Lehnertz, K., Elger, C.E. 2003 Epileptic seizures are preceded by a decrease in synchronization. *Epilepsy Res.* **53(3)**, 173-185.

[33] Ramgopal, S., Thome-Souza, S., Jackson, M., Kadish, N.E., Fernández, I.S., Klehm, J., Bosl, W., Reinsberger, C., Schachter, S., Loddenkemper, T. 2014 Seizure detection, seizure prediction, and closed-loop warning systems in epilepsy. *Epilepsy Behav.* **37**, 291-307.

[34] Dadok, V., Kirsch, H.E., Sleigh, J.W., Lopour, B.A., Szeri, A.J. 2015 A probabilistic method for determining cortical dynamics during seizures. *To appear in J. Comput. Neurosci.*

[35] Doedel, E.J., Champneys, A.R., Dercole, F., Fairgrieve, T., Kuznetsov, Y., Oldeman, B., Paffenroth, R., Sandstede, B., Wang, X., Zhang, C. 2008 *AUTO-07P: Continuation and Bifurcation Software for Ordinary Differential Equations*.

[36] Green, K.R., van Veen, L. 2012 Open-source tools for dynamical analysis of Lileys mean-field cortex model. *J. Comput. Sci.* **5**(3), 507-516.

[37] Marreiros, A.C, Daunizeau, J., Kiebel, S.J., Friston, K.J. 2008 Population dynamics: Variance and the sigmoid activation function. *Neuroimage* **42**, 147-157.

[38] Deisseroth, K. 2011 Optogenetics. *Nat. Methods* **8**, 26-29.

[39] Cossart, R., Dinocourt, C., Hirsch, J.C., Merchan-Perez, A., De Felipe, J., Ben-Ari, Y., Esclapez, M., Bernard, C. 2001 Dendritic but not somatic GABAergic inhibition is decreased in experimental

epilepsy. *Nat. Neurosci.* **4**(1), 52-62.

[40] Cobos, I., Calcagnotto, M.E., Vilaythong, A.J., Thwin, M.T., Noebels, J.L., Baraban, S.C., Rubenstein, J.L. 2005 Mice lacking Dlx1 show subtype-specific loss of interneurons, reduced inhibition and epilepsy. *Nat. Neurosci.* **8**(8), 1059-1068.

[41] Nagel, G., Szellas, T., Huhn, W., Kateriya, S., Adeishvili, N., Berthold, P., Ollig, D., Hegemann, P., Bamberg, E.: Channelrhodopsin-2, a directly light-gated cation-selective membrane channel. Proceedings of the National Academy of Sciences **100(24)**, 13,940–13,945 (2003)

[42] Chuong, A. S., Miri, M. L.*, Busskamp, V.*, Matthews, G.A.C.*, Acker, L.C.*, Soresnsen, A.T., Young, A., Klapoetke, N. C., Henninger, M.A., Kodandaramaiah, S.B., et al. 2014 Noninvasive optical inhibition with a red-shifted microbial rhodopsin. *Nat. Neurosci.* **17**, 1123-1129.

[43] Kawaguchi, Y., Kubota, Y. 1997 GABAergic cell subtypes and their synaptic connections in rat frontal cortex. *Cereb. Cortex* **7**(6), 476-486.

[44] Cauli, B., Audinat, E., Lambolez, B., Angulo, M.C., Ropert, N., Tsuzuki, K., Hestrin, S., Rossier, J. 2014 Molecular and physiological diversity of cortical nonpyramidal cells. *J. Neurosci.* **17**(10), 3894-3906.

[45] Rudy, B., Fishell, G., Lee, S., Hjerling-Leffler, J. 2011 Three groups of interneurons account for nearly 100% of neocortical GABAergic neurons. *Dev. Neurobiol.* **71**(1), 45-61.

[46] Berthold, P., Tsunoda, S.P., Ernst, O.P., Mages, W., Gradmann, D., Hegemann, P. 2008 Channelrhodopsin-1 initiates phototaxis and photophobic responses in chlamydomonas by immediate light-induced depolarization. *Plant Cell* **20**, 16651677.

[47] Zhang, F., Prigge, M., Beyriere, F., Tsunoda, S.P., Mattis, J., Yizhar, O., Hegemann, P., Deisseroth, K. 2008 Red-shifted optogenetic excitation: a tool for fast neural control derived from Volvox carteri. *Nat. Neurosci.* **11(6)**, 631-633.

[48] Tsunoda S.P., Hegemann P. 2009 Glu 87 of channelrhodopsin-1 causes pH-dependent color tuning and fast photocurrent inactivation. Photochem Photobiol.**85**, 564569.